ELSEVIER

Journal of Crystal Growth 211 (2000) 257–264

JOURNAL OF CRYSTAL GROWTH

www.elsevier.nl/locate/jcrysgro

Phase-matched crystal growth of $AgGaSe_2$ and $AgGa_{1-x}In_xSe_2$

Peter G. Schunemann*, Scott D. Setzler, Thomas M. Pollak

Sanders, A Lockheed Martin Company, MER15-1813, P.O. Box 868, Nashua, NH 03061-0868, USA

Abstract

$AgGaSe_2$ and $AgGa_{1-x}In_xSe_2$ single crystals have been grown by the horizontal gradient freeze technique directly along the phase-matching orientation required for frequency-doubling the output of a 9.27 μm CO_2 laser. Samples for second harmonic generation exceeding 55 mm in length have been fabricated from 19 mm-diameter boules with minimal waste. Low-loss $AgGaSe_2$ samples (after annealing in Ag_2Se) generated over 3 W of 4.6 μm output at external efficiencies of 26%. $AgGa_{1-x}In_xSe_2$ crystals were grown with In concentrations between $x = 0.37$ and 0.42, and were free of the Ga_2Se_3-rich precipitates that normally plague as-grown $AgGaSe_2$. Non-critically phase-matched second harmonic generation was successfully demonstrated in the sample grown from a melt with $x = 0.42$.

1. Introduction

$AgGaSe_2$ is the nonlinear optical material of choice for frequency-doubling the output of CO_2-lasers into mid-infrared spectral range [1]. In order to satisfy the conditions for phase matching as well as maximize the effective nonlinear optical coefficient, device crystals must be cut from (1 1 0) slabs at an angle of 47.3° from the *c*-axis [2]. Substituting approximately 40% In for Ga shifts this phase matching angle to 90° to achieve a condition known as non-critical phase matching (NCPM) which dramatically enhances the conversion efficiency [2–4]. In either case (but particularly for $AgGa_{1-x}In_xSe_2$), it would be advantageous to grow the crystal directly along the orientation required for device crystals (i.e., "phase-matched" crystal growth) to allow for fabrication of long samples (since conversion efficiency scales as the length *squared*) without scaling the growth process to larger diameters. $AgGaSe_2$ and $AgGa_{1-x}In_xSe_2$ have been grown previously by the vertical Bridgman technique [5–8], which requires that growth be seeded along the *c*-axis to allow for unconstrained vertical expansion of the *c*-axis during cooling, as shown in Fig. 1a. Here we report "phase-matched" growth (i.e., seeded growth along the specific orientation required for birefringent phase matching, illustrated in Fig. 1b and c) of $AgGaSe_2$ and $AgGa_{1-x}In_xSe_2$ using the horizontal gradient freeze (HGF) technique.

2. Crystal growth

2.1. Feed purification and synthesis

$AgGaSe_2$ and $AgGa_{1-x}In_xSe_2$ polycrystalline ingots were synthesized by direct reaction of the elements using high-purity starting materials.

* Corresponding author. Tel.: +1-603-885-5041; fax: +1-603-885-0207.

E-mail address: peter.g.schunemann@lmco.com (P.G. Schunemann)

0022-0248/00/$ - see front matter
PII: S0022-0248(99)00855-6

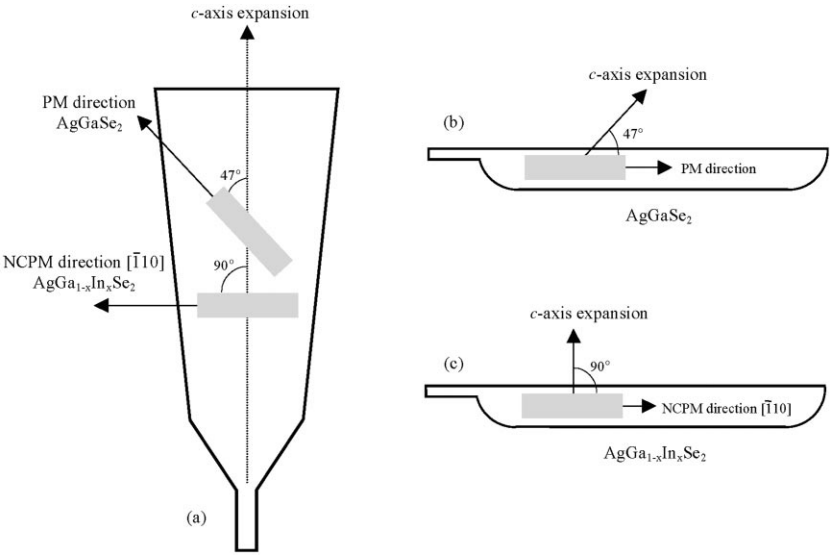

Fig. 1. (a) Orientation of 9.27 μm-pumped SHG samples cut from a *c*-axis $AgGaSe_2$ or $AgGa_{1-x}In_xSe_2$ crystal grown by vertical Bridgman; (b and c) phase-matched crystals grown by HGF. (In each case, the [1 1 0] plane lies in the page.)

Seven-nines liquid Ga (Rhone-Pollenc) and six-nines In shot (Johnson Matthey) were used as received. Six-nines Ag shot (Johnson Matthey) was vacuum-baked in an isothermal furnace at 350°C to remove any tarnish from the as-received pellets. Finally, five-nines Se (Metal Specialties) was vacuum distilled at 650°C.

After purification, the elements were weighed in stoichiometric amounts into a high-walled, uncoated fused-silica boat which was then encapsulated in an evacuated quartz ampoule and loaded into a horizontal rocking furnace fitted with a sodium-filled inconel heat pipe. The ampoule was then heated at 100°C/h to 650°C, 20°C/h to 950°C, rocked for 24 h, and cooled at 300°C/h to room temperature. (The $AgGaSe_2$ synthesis runs, as well as the early $AgGa_{1-x}In_xSe_2$ runs, were performed without rocking, but in the case of $AgGa_{1-x}In_xSe_2$ these yielded inhomogeneous starting materials which adversely affected crystal growth.) The resulting 100-g charges were shiny and free of any visible surface contamination (i.e., "scum").

2.2. Horizontal gradient freeze growth

HGF growth of $AgGaSe_2$ and $AgGa_{1-x}In_xSe_2$ was performed using a two-zone transparent furnace [9,10]. The viewing capability provided by the transparent furnace greatly facilitated the seeding process, and allowed in situ monitoring of the crystal quality and the solid–liquid interface shape. (Polycrystallinity manifested itself as irregularities in the surface of the solidified crystal and/or as a discontinuity in the shape of the solid–liquid interface. When observed, the crystal could be melted back and regrown without wasting weeks of valuable process time.) Low axial temperature gradients were used to suppress vapor transport of volatile species and to minimize stresses related to anisotropic thermal expansion.

The pre-synthesized polycrystalline ingot was first loaded into a vitreous carbon, PBN, or PBN-coated graphite boat with a vertically tapered channel at one end that held an oriented seed crystal. (In the case of $AgGaSe_2$, a 1.3 mol% excess of Se was also added.) The orientation of the seed crystal is shown in Fig. 1: the side faces corresponded to (1 1 0) planes and the *c*-axis was vertical at an angle of 47.3° for $AgGaSe_2$ and 90° for $AgGa_{1-x}In_xSe_2$. (90° $AgGaSe_2$ seeds were used for the first $AgGa_{1-x}In_xSe_2$ growth experiments until single-crystal seeds could be cut from the quaternary itself.) After weighing, the boat was loaded into a fused silica ampoule which was back-filled with

argon (enough to generate an inert over-pressure of ~1 atm during growth), encapsulated, and heated in the two-zone transparent furnace. The temperatures of the two zones were adjusted to give an axial gradient of 2–2.5°C/cm. Melting commenced in the hot zone at the tail end of the boat, and continued as the temperature was gradually raised until the tip of the seed was melted. Both zones were then cooled simultaneously at 0.05–0.25°C/h to produce directional solidification at 0.25–1 mm/h.

During growth, the solid–liquid interface was observed to be slightly concave toward the melt for both compounds. The solid–liquid interface was smooth throughout the $AgGaSe_2$ runs, but in the early $AgGa_{1-x}In_xSe_2$ growth runs it became extremely rough after 1–2 cm of growth (evidence of interface breakdown due to constitutional supercooling) resulting in severe polycrystallinity and cracking. By thoroughly mixing the starting material in a rocking furnace during synthesis, and by reducing the growth rate to below 0.5 mm/h, this interface breakdown was eliminated until the very last-to-freeze portion of the boule.

Low axial temperature gradients, combined with an over-pressure of argon, kept vapor losses to a minimum. Only 0.2 g on average were lost over the course of a $AgGaSe_2$ growth run, which was more than compensated by the excess Se added to the melt. In the case of $AgGa_{1-x}In_xSe_2$ the ampoule was completely free of vapor deposits since the addition of a fourth component lowered the individual activity of each element in the melt, significantly reducing the total vapor pressure over the quaternary. It is interesting to note, however, that the surface of the growing crystal was covered by a thin liquid layer extending approximately 2 cm behind the growth interface, suggesting some interaction with the vapor phase.

Once the melt was fully solidified, the furnace was cooled at 35°C/h to room temperature. A typical $AgGaSe_2$ crystal, measuring 19 mm in diameter by 140 mm in length, is shown in Fig. 2. The final few centimeters are characterized by polycrystallinity and cracking due to the appearance of eutectic phases. Otherwise, the boule is crack-free and monocrystalline, yielding at least two (and up to six) $6 \times 6 \times 40\ mm^3$ samples oriented for 9.27-μm-pumped SHG as shown. $AgGa_{1-x}In_xSe_2$ boules were similar in appearance except for longer polyphase regions (up to 3 or 4 cm) at the end of boule. The $AgGa_{1-x}In_xSe_2$ crystals were also somewhat more prone to cracking, which was minimized by slower post-growth cooling (17°C/h).

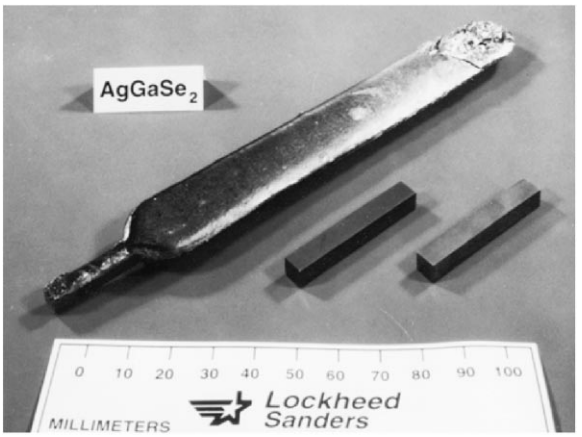

Fig. 2. Phase-matched $AgGaSe_2$ single crystal boule and 40 mm-long SHG samples for 9.27 μm CO_2 laser pumping.

At total of 50 $AgGaSe_2$ growth experiments were conducted. Once the baseline process was established, the overall single crystal yield was 80%. Only 12 $AgGa_{1-x}In_xSe_2$ runs were made. The first five runs were conducted at an indium concentration of $x = 0.37$, and yielded single crystal grains of sufficient size to provide seed crystals and preliminary laser test specimens. The next seven growth runs were devoted to the remaining five compositions in the series: $x = 0.38$, 0.39, 0.40, 0.41, and 0.42. The orientation of the phase-matched seed crystal was reproduced in every run except one, resulting in crack-free single crystals across the full diameter and extending up to 100 mm in length.

3. Thermal expansion

Linear thermal expansion coefficients were measured both parallel and perpendicular to the c-axis on HGF-grown $AgGaSe_2$ and $AgGa_{1-x}In_xSe_2$ samples using a TA Instruments model 943 thermomechanical analyzer. The 6.76 (c-axis) × 5.06 × 4.70 mm^3 $AgGaSe_2$ sample was cut with $\{0\,0\,1\}$

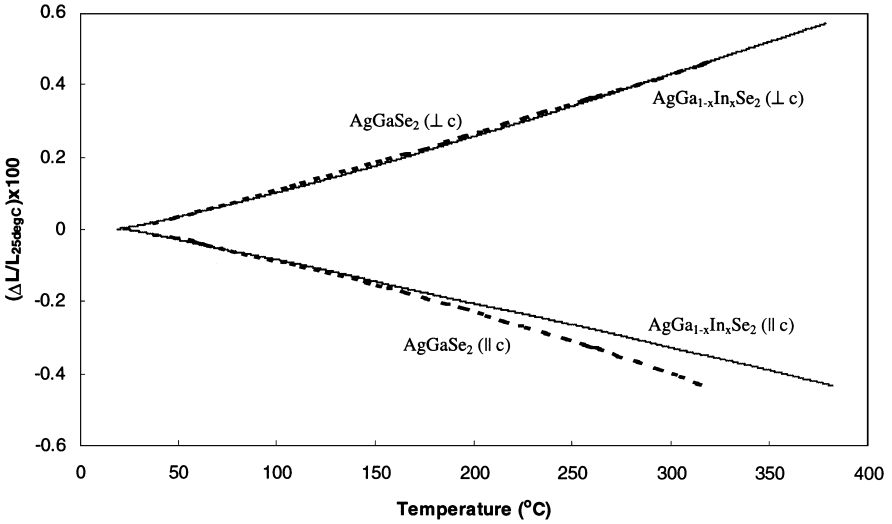

Fig. 3. Thermal expansion of $AgGaSe_2$ and $AgGa_{1-x}In_xSe_2$ ($x = 0.42$) parallel and perpendicular to the c-axis.

and $\{1\,1\,0\}$ faces from an as-grown, crack-free single crystal. The $AgGa_{1-x}In_xSe_2$ sample was cut from a crystal with a starting composition $x = 0.42$ and measured 6.94 mm along the (0 0 1) dimension, and 6.41 mm × 4.78 mm along the two (1 1 0) dimensions. Expansion was measured between 25°C and 350°C (300°C for $AgGaSe_2$) at a heating rate of 5°C/min. Linear fits to the data, which are plotted in Fig. 3, yielded the following values for the thermal expansion coefficient α: for $AgGaSe_2$, $\alpha = -15.7 \times 10^{-6}\ ^{\circ}C^{-1}$ parallel to c and $\alpha = 16.3 \times 10^{-6}\ ^{\circ}C^{-1}$ perpendicular to c; for $AgGa_{0.58}In_{0.42}Se_2$, $\alpha = -12.1 \times 10^{-6}\ ^{\circ}C^{-1}$ parallel to c and $\alpha = 16.8 \times 10^{-6}\ ^{\circ}C^{-1}$ perpendicular to c. The values perpendicular to c are nearly equivalent and in good agreement with the data of Iseler [6]. Our value for the negative c-axis expansion coefficient of $AgGaSe_2$, reproducible over numerous measurements, is nearly twice that measured by Iseler [6], and ~50% larger than for the quaternary (at $x = 0.42$). We therefore attribute the greater tendency of $AgGa_{1-x}In_xSe_2$ toward cracking during cool-down to variations in thermal expansion due to compositional inhomogeneity, especially since cracking was most common at the ends of the boule where the compositional variations are more severe.

4. Absorption and scattering losses

Near-infrared absorption spectra for HGF-grown $AgGaSe_2$ and $AgGa_{1-x}In_xSe_2$ were measured between 0.6 and 3.0 μm using a Perkin Elmer Lambda 9 UV/VIS/NIR spectrophotometer, and were corrected for surface reflection losses as a function of wavelength using the Sellmeier coefficients listed in Table 1. Data for as-grown $AgGaSe_2$ and $AgGa_{1-x}In_xSe_2$ ($x = 0.42$) are shown in Fig. 4. The high losses in the as-grown $AgGaSe_2$ sample are the result of scattering from needle-like Ga_2Se_3-rich ($AgGa_7Se_{11}$) precipitates which form as a result of an off-stoichiometric congruency (which causes all $AgGaSe_2$ crystals to grow slightly rich in Ga_2Se_3) and retrograde solubility (which causes the excess Ga_2Se_3 to precipitate upon cooling) in the Ag_2Se–Ga_2Se_3 pseudobinary system [7,11,12]. Note that these scattering losses have been dramatically reduced in the as-grown $AgGa_{1-x}In_xSe_2$ crystal, and IR microscopy confirmed the absence of any needle-like precipitates.

It is well known that the Ga_2Se_3-rich scattering centers in $AgGaSe_2$ can be eliminated by annealing in the presence of Ag_2Se [7,12]. We found that annealing at 800°C for 14 days in direct contact with Ag_2Se powder (evenly distributed over the top

Table 1
Sellmeier coefficients for $AgGaSe_2$ and $AgInSe_2$, where $n^2 = A + B\lambda^2/(\lambda^2 - C) + D\lambda^2/(\lambda^2 - E)$, fit to the refractive index data of Boyd et al. [16].[a]

		A	B	C	D	E
$AgGaSe_2$	o	4.08904	2.76132	0.15669	11.72170	9502.60
	e	4.44502	2.23490	0.20592	8.64984	7054.40
$AgInSe_2$	o	5.39323	1.58209	0.42109	4.83368	5535.43
	e	5.47808	1.51350	0.49571	5.13294	5535.43
$AgGa_{0.58}In_{0.42}Se_2$	o	4.63680	2.26604	0.26774	8.82873	7836.39
	e	4.87891	1.93191	0.33763	7.17274	6416.43

[a] Values for $AgGa_{0.58}In_{0.42}Se_2$ were determined by linear interpolation. (o) ordinary polarization ($E \perp c$), (e) extra-ordinary polarization ($E \| c$).

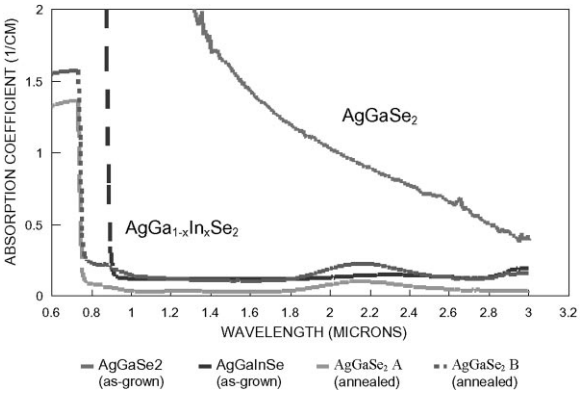

Fig. 4. Near infrared absorption spectra of as-grown $AgGaSe_2$, as-grown $AgGa_{1-x}In_xSe_2$ ($x = 0.42$), and two annealed $AgGaSe_2$ crystals.

and bottom surfaces of the $AgGaSe_2$ crystal) was far more effective than non-contact annealing. Experiments using 1.0, 1.25, and 1.5 mol% excess Ag_2Se indicated that 1.25 mol% yielded the best results. We also found that growth from a slight excess of Se ($\sim$1.3 mol%) benefited the clearing process during annealing. When an over-pressure of Se (0.2 atm) was introduced during annealing, however, a sharp absorption peak appeared at 4.6 μm (This was extremely undesirable, since it coincided almost exactly with the second harmonic output wavelength.) We have also observed this 4.6-μm peak in a few isolated crystals from a commercial source, and in two of the spectra published in Ref. [13] from the same source, but no mention of its existence nor its origin has been previously reported.

Fig. 4 shows the extraordinary-polarized ($E \| c$) absorption spectra for two $AgGaSe_2$ crystals after annealing. The first (sample A) represents the best HGF-grown material achieved to date, with absorption coefficients of 0.003 and 0.007 cm^{-1} at 9.27 and 4.635 μm, respectively. The second (sample B) was cut from a $AgGaSe_2$ boule which contained a central core of melt inclusions after an initial 3–4 cm of inclusion-free growth. The second-phase precipitates were completely removed by the annealing process, but inspection with an infrared microscope revealed residual 30-μm-sized spherical inclusions that could not be removed by annealing. (The composition of these inclusions was measured by electron microprobe to be nearly identical to the matrix composition, suggesting they are entrapped-melt droplets.) These inclusions were responsible for residual scattering losses of $\sim$0.10 cm^{-1}. Similar melt inclusions were present in varying degrees in all the $AgGa_{1-x}In_xSe_2$ crystals: we hope to eliminate these in future experiments by improved mixing both prior to and during the growth process.

The final notable feature of the spectra in Fig. 4 is the presence of a small but significant e-polarized absorption peak centered around 2.2 μm. This absorption band, combined with the low thermal conductivity of $AgGaSe_2$, leads to severe thermal lensing in high-power 2.05-μm-pumped optical parametric oscillators [14]. Halliburton et al. [15] used electron paramagnetic resonance to identify

Ni^{+} impurities (present at levels on the order of 10^{17} cm^{-3}) as the source of this absorption, and we recently confirmed this assignment by intentionally doping with $2\times10^{19}cm^{-3}$ (1950 ppm) Ni, which increased the 2.2 μm absorption by over two orders of magnitude. Note that the e-polarized spectrum for $AgGa_{1-x}In_xSe_2$ shows barely a hint of an absorption peak in this region (although the residual scattering may still mask a small peak). This suggests that perhaps Ga is the source of the Ni impurities in $AgGaSe_2$. A more likely possibility is that slight differences in Se stoichiometry shifted most of the Ni impurities in $AgGa_{1-x}In_xSe_2$ into a non-absorbing valence state (i.e., Ni^{2+} or Ni^{3+}).

5. Second harmonic generation

Phase-matched crystal growth of $AgGaSe_2$ and $AgGa_{1-x}In_xSe_2$ using the HGF technique allowed for simplified fabrication of long ($\geqslant 40$ mm) SHG samples with minimal material waste. $6\times6\times40$ mm^3 $AgGaSe_2$ device crystals were cut from annealed boule sections, and the end faces were polished and anti-reflection (AR) coated for minimum reflectance ($<0.5\%$) at 9.27 and 4.635 μm (see Fig. 2). Pumping with 11.8 W of average input power from a pulsed CO_2 laser (10 ns pulsewidth, 100 kHz repetition rate) into a 200-μm-diameter spot focused at the center of the crystal produced 3.05 W of second harmonic output (at 26% conversion efficiency).

The same pump laser was used to test a series of $AgGa_{1-x}In_xSe_2$ samples to determine the experimental In concentration required for NCPM. (Linear interpolation of the Sellmeier coefficients in Table 1 predicts NCPM at $x=0.394$). SHG samples were cut and polished with apertures >1 cm^2 and lengths up to 55 mm. Two attempts were made to apply AR coatings, but the large thermal expansion across one dimension of the face, combined with a large contraction across the opposite dimension, caused the coatings to peel in both instances. Samples cut from boules with initial In fractions x equal to 0.37, 0.39, 0.40, 0.41, and 0.42 were evaluated. NCPM was achieved in a 40.7-mm-long sample cut from the first-to-freeze end of the crystal grown with $x=0.42$. The external conversion efficiency was limited to 1.8% (125 mW output for 6.92 W of pump) due to surface reflection (peeled coatings) and internal scattering losses (inclusions). These losses were insufficient to completely account for the low efficiency, however, suggesting that compositional non-uniformity may also be an important factor limiting the performance of $AgGa_{1-x}In_xSe_2$.

6. Compositional uniformity

One of the key issues in using mixed crystals to "engineer" the birefringence for non-critical phase-matching is whether sufficient compositional uniformity can be achieved to maintain a constant phase-matching angle of 90° along the entire sample length. In this case, too low of an In concentration will shift the phase matching angle below 90°, whereas too high a value will stop frequency conversion completely. We therefore measured the indium concentration along each boule using a JEOL JXA-733 electron probe microanalyzer at the MIT Dept. of Earth, Atmospheric, and Planetary Sciences. The results for a representative $AgGa_{1-x}In_xSe_2$ boule ($x=0.40$) are plotted in Fig. 5 as mol% $AgInSe_2$ versus distance (cm) from the seed (a) and from the center (b) to demonstrate the axial and radial segregation, respectively. Within the accuracy of the measurement ($\pm$ 1.7%), the axial segregation data agree well with a normal freezing distribution fit to an In segregation coefficient $k=0.85$. (Data for four other boules ranging from $x=0.37$ to 0.42 yielded reasonable fits using the same value for k.) The radial In distribution was more uniform, and could be modeled using an effective k value near unity ($k=0.98$).

Electron microprobe results on the NCPM sample grown with $x=0.42$ indicated a center composition of 37.8% In which varied between 37.1% and 38.6% over its 40.7 mm length. This composition is significantly lower than the 39.4% value predicted by our Sellmeier fits (although within the error of the microprobe measurement), and even further below the 42.2% value predicted in Ref. [4]. More carefully calibrated microprobe measurements, combined with more extensive

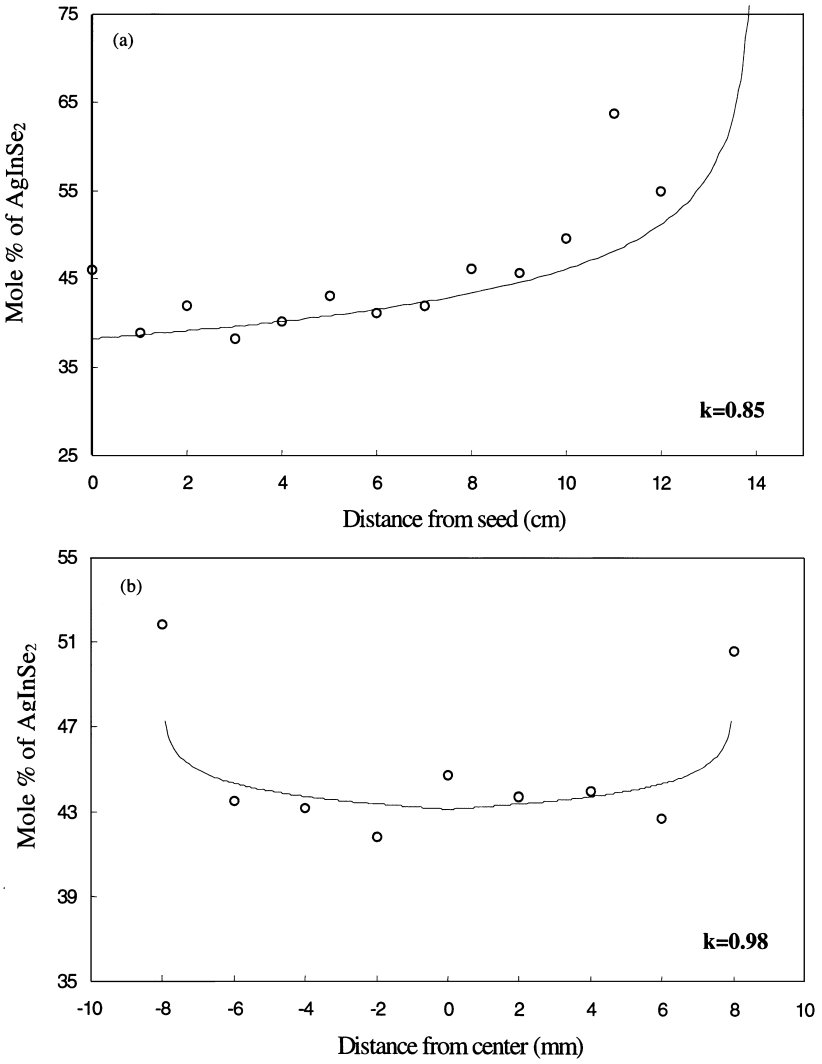

Fig. 5. In content (plotted as mol% $AgInSe_2$) measured by electron microprobe: (a) along the length of the boule, and (b) across the diameter of the boule (at the 8 cm position).

SHG testing, will be required to accurately define the In composition for NCPM.

Acknowledgements

The authors gratefully acknowledge Dr. Norman Barnes at the NASA Langley Research Center for providing the Sellmeier fits in Table 1.

References

[1] P.G. Schunemann, K.L. Schepler, P.A. Budni, MRS Bull. 23 (1998) 45.
[2] P.G. Schunemann, D.M. Rines, T.M. Pollak, Conference on Lasers and Electro-Optics, Vol. 6, 1998 OSA Technical Digest Series, Optical Society of America, Washington, DC, 1998, p. 271.
[3] G.C. Bhar, S. Das, D.V. Satyanarayan, P.K. Datta, U. Nundi, Yu.N. Andreev, Opt. Lett. 20 (1995) 2057.

[4] E. Takaoka, K. Kato, Opt. Lett. 24 (1999) 902.
[5] R.K. Route, R.S. Feigelson, J. Crystal Growth 24/25 (1974) 390.
[6] G.W. Iseler, J. Crystal Growth 41 (1977) 146.
[7] R.S. Feigelson, R.K. Route, Opt. Eng. 26 (1987) 113.
[8] V.V. Badikov, V.B. Laptev, V.L. Panyutin, E.A. Ryabov, G.S. Shevyrdyaeva, O.B. Shcherbina, Sov. J. Quantum Electron. 22 (1992) 722.
[9] P.G. Schunemann, T.M. Pollak, US Patent No. 5,611,856, March 18, 1997.
[10] P.G. Schunemann, T.M. Pollak, MRS Bull. 23 (1998) 23.
[11] J.C. Mikkelsen Jr., Mater. Res. Bull. 12 (1977) 497.
[12] R.K. Route, R.S. Feigelson, R.J. Raymakers, M.M. Choy, J. Crystal Growth 33 (1976) 239.
[13] B.C. Ziegler, K.L. Schepler, Appl. Opt. 30 (1991) 5077.
[14] G.C. Catella, L.R. Shiozawa, J.R. Hietenan, R.C. Eckardt, R.K. Route, R.S. Feigelson, D.G. Cooper, C.L. Marquardt, Appl. Opt. 32 (1993) 3948.
[15] L.E. Halliburton, N.C. Giles, P.G. Schunemann, T.M. Pollak, J. Appl. Phys. 79 (1996) 556.
[16] G.D. Boyd et al., IEEE J. Quantum Electron QE8 (1972) 419.